HHS Public Access

Author manuscript

Nat Immunol. Author manuscript; available in PMC 2018 January 16.

Published in final edited form as:

Nat Immunol. 2017 December ; 18(12): 1332–1341. doi:10.1038/ni.3868.

Oxidative stress controls regulatory T cell apoptosis and suppressor activity and PD-L1-blockade resistance in tumor

Tomasz Maj[1,9], **Wei Wang**[1,2,9], **Joel Crespo**[1,3], **Hongjuan Zhang**[1], **Weimin Wang**[1,4], **Shuang Wei**[1], **Lili Zhao**[5], **Linda Vatan**[1], **Irene Shao**[1], **Wojciech Szeliga**[1], **Costas Lyssiotis**[6,7], **J Rebecca Liu**[4], **Ilona Kryczek**[1], and **Weiping Zou**[1,3,7,8]

[1]Department of Surgery, University of Michigan School of Medicine, Ann Arbor, Michigan, USA

[2]Department of Immunology and Key Laboratory of Medical Immunology of the Ministry of Public Health, School of Basic Medical Sciences, Peking University Health Science Center, Beijing, China

[3]Rackham Graduate School, University of Michigan, Ann Arbor, Michigan, USA

[4]Department of Obstetrics and Gynecology, University of Michigan School of Medicine, Ann Arbor, Michigan, USA

[5]Department of Biostatistics, University of Michigan School of Medicine, Ann Arbor, Michigan, USA

[6]Department of Molecular and Integrative Physiology, University of Michigan School of Medicine, Ann Arbor, Michigan, USA

[7]The University of Michigan Comprehensive Cancer Center, University of Michigan, Ann Arbor, Michigan, USA

[8]Department of Pathology, University of Michigan School of Medicine, Ann Arbor, Michigan, USA

Abstract

Live regulatory T cells (T_{reg} cells) suppress antitumor immunity, but how T_{reg} cells behave in the metabolically abnormal tumor microenvironment remains unknown. Here we show that tumor T_{reg} cells undergo apoptosis, and such apoptotic T_{reg} cells abolish spontaneous and PD-L1-blockade-mediated antitumor T cell immunity. Biochemical and functional analyses show that adenosine, but not typical suppressive factors such as PD-L1, CTLA-4, TGF-β, IL-35, and IL-10, contributes

Correspondence should be addressed to W.Z. (wzou@med.umich.edu).

[9]These authors contributed equally to this work.

AUTHOR CONTRIBUTIONS

T.M., Wei Wang, I.K., and W.Z. designed the experiments. T.M., I.K., and W.Z. wrote the paper. Wei Wang, T.M., J.C., S.W., L.V., and I.K. performed the *in vivo* tumor experiments. L.V., W.S., I.K., and J.R.L. provided and processed clinical specimens and performed immunohistochemical and pathological analysis. T.M., Wei Wang, H.Z., I.S., and Weimin Wang performed the immunological and biochemical assays. I.K., L.Z., T.M., C.L., Wei Wang and W.Z. analyzed data.

COMPETING FINANCIAL INTERESTS

The authors declare no competing financial interests.

Note: Any Supplementary Information and Source Data files are available in the online version of the paper.

to apoptotic T_{reg}-cell-mediated immunosuppression. Mechanistically, apoptotic T_{reg} cells release and convert a large amount of ATP to adenosine via CD39 and CD73, and mediate immunosuppression via the adenosine and A_{2A} pathways. Apoptosis in T_{reg} cells is attributed to their weak NRF2-associated antioxidant system and high vulnerability to free oxygen species in the tumor microenvironment. Thus, the data support a model wherein tumor T_{reg} cells sustain and amplify their suppressor capacity through inadvertent death via oxidative stress. This work highlights the oxidative pathway as a metabolic checkpoint that controls T_{reg} cell behavior and affects the efficacy of therapeutics targeting cancer checkpoints.

Extensive studies have been conducted to define the development, conversion, stability, and regulatory mechanisms of $CD4^+Foxp3^+$ T_{reg} cells in homeostasis and a variety of disease models[1–10]. It is well known that T_{reg} cells are recruited into the tumor microenvironment and act as one of the major immunosuppressors dampening spontaneous tumor-associated antigen (TAA)-specific T cell immunity[4–6], as well as immunotherapy-induced and active-vaccination-induced antitumor immunity[5,6]. However, how T_{reg} cells behave in the metabolically abnormal tumor microenvironment remains unknown.

The Warburg effect is an important metabolic feature in many types of cancer[11]. Recent studies indicate that glycolysis regulates T cell activation and effector function[12,13]. Given that glucose, among other nutrients, is poorly replenished in tumors, it is assumed that T cell glycolytic metabolism is altered as a result of the Warburg effect in the tumor microenvironment[13–16]. In support of this, poor glycolysis can alter effector memory T cell function in the tumor microenvironment[14,16]. In addition, oxygen-sensing prolyl-hydroxylase proteins[17], potassium ions released from necrotic cells[18], and abnormal zinc metabolism[19] can impair effector T cell function in the tumor microenvironment. These findings underscore the significance of the metabolic regulation of memory T cells in tumors.

The homeostatic balance between T_{reg} cells and T helper cells may be metabolically regulated in mice[20–23]. However, T_{reg} cells adopt memory and effector phenotypes in the human tumor microenvironment[4,24]. It is unknown whether T_{reg} cells are subject to glycolytic regulation in tumors. Furthermore, oxidative stress is an additional metabolic feature in the tumor microenvironment. Recent studies have shown that myeloid dendritic cells (DCs) are phenotypically and functionally altered by oxidative stress in the tumor microenvironment[25]. However, it is unknown whether oxidative stress alters T_{reg} cell phenotype and function in tumors.

To address these questions, we examined the phenotypic and functional nature of T_{reg} cells in the tumor microenvironment in human ovarian cancer and in several types of mouse cancer, and investigated the mechanisms and roles of metabolism in shaping the biological behaviors of T_{reg} cells. We observed that T_{reg} cells were highly apoptotic in the tumor microenvironment, and that apoptotic T_{reg} cells achieved superior suppressor function via an oxidative-stress-associated mechanism. Furthermore, we found that oxidative stress, rather than glycolysis, was the metabolic mechanism that controlled tumor T_{reg} cell functional behavior and tempered the therapeutic efficacy of immune checkpoint therapy.

RESULTS

High T_{reg} cell apoptosis in the tumor microenvironment

A previous study showed that T_{reg} cells are recruited into the human tumor microenvironment and inhibit TAA-specific T cell immunity[4]. However, it is unknown how T_{reg} cells behave in the metabolically abnormal tumor microenvironment. To investigate this, we used polychromatic flow cytometry analysis (Supplementary Fig. 1a) to analyze cell proliferation and apoptosis in primary $Foxp3^+$ T_{reg} cells and conventional $Foxp3^-CD4^+$ T cells in human ovarian cancer tissues. We found that T_{reg} cells expressed higher levels of the cell cycle protein Ki67 than conventional T cells did in the human ovarian cancer microenvironment (Supplementary Fig. 1b). In addition, flow cytometry analyses showed that T_{reg} cells underwent substantial apoptosis compared with $Foxp3^-$ conventional T cells in primary and metastatic ovarian cancer tissues, as determined on the basis of cleaved caspase-3 expression (Fig. 1). Immunofluorescence staining demonstrated the colocalization of Foxp3 and cleaved caspase-3 in ovarian cancer tissues (Fig. 1c and Supplementary Fig. 1c). We quantified proapoptotic and antiapoptotic gene transcripts in human ovarian-cancer-infiltrating T_{reg} cells and conventional T cells. T_{reg} cells expressed high levels of proapoptotic gene transcripts (Fig. 1d) and low levels of antiapoptotic gene transcripts (Fig. 1e) compared with conventional T cells in the same human ovarian cancers. We obtained similar results in mice with ID8 ovarian cancer, MC38 colon cancer, and B16 melanoma (Fig. 1f,g). Furthermore, using gene set enrichment analysis, we found enriched expression of apoptotic genes in infiltrating T_{reg} cells in mouse B16 melanoma (Fig. 1h and Supplementary Tables 1 and 2) in the GEO database (GSE55705)[26]. In mouse T_{reg} cells cultured with MC38 tumor media, we detected increased expression of proapoptotic genes (Supplementary Fig. 1d) and decreased expression of antiapoptotic genes (Supplementary Fig. 1e). Thus, the data indicate that T_{reg} cells are highly apoptotic in the tumor microenvironment.

Apoptotic T_{reg} cells mediate superior immunosuppression

Foxp3 controls T_{reg} cell development and functional integrity[1,2]. Live T_{reg} cells inhibit TAA-specific T cell activation[4,6,27]. It is unknown whether apoptotic T_{reg} cells are functionally suppressive. To test this, we isolated infiltrating T_{reg} cells from human ovarian cancer samples, induced their apoptosis with anti-Fas monoclonal antibody (mAb) (Supplementary Fig. 2a), and examined their suppressor activity. Apoptotic T_{reg} cells inhibited the expression of interferon-γ (IFN-γ) and tumor necrosis factor (TNF) in $CD4^+$ and $CD8^+$ T cells (Fig. 2a). When we compared the suppressor activities of live and apoptotic infiltrating T_{reg} cells and apoptotic conventional T cells in human ovarian cancer, we found that apoptotic T_{reg} cells were more efficient than live T_{reg} cells at inhibiting T cell IL-2 production (Fig. 2b). Thus, human-cancer-associated apoptotic T_{reg} cells are potent immune suppressors.

Next, we carried out similar experiments with T_{reg} cells from healthy mice and tumor-bearing mice. As expected, in the *in vitro* T cell suppressive assay, live T_{reg} cells from healthy mice inhibited T cell cytokine production (Supplementary Fig. 2b,c). We induced T_{reg} cell apoptosis with irradiation, serum starvation, fluorouracil, and anti-Fas mAb. Similar

to what we observed in human apoptotic T_{reg} cells (Fig. 2b), regardless of how T_{reg} cell apoptosis was induced, mouse apoptotic T_{reg} cells were superior at suppressing the expression of T cell TNF and IL-2 compared with identical amounts of normal live T_{reg} cells (Supplementary Fig. 2b,c). We further compared the suppressor activities of live and apoptotic mouse MC38-tumor-infiltrating T_{reg} cells. Again, apoptotic mouse tumor-infiltrating T_{reg} cells were more potent suppressors than live T_{reg} cells (Fig. 2c). Furthermore, mouse apoptotic tumor-infiltrating T_{reg} cells, rather than apoptotic tumor-infiltrating conventional T cells, strongly inhibited T cell IL-2 production (Fig. 2d). Thus, mouse tumor-associated apoptotic T_{reg} cells are powerful immune suppressors.

In addition to *in vitro* and *ex vivo* suppressor activity, we studied whether apoptotic T_{reg} cells suppress tumor immunity *in vivo*, using three systems: (i) spontaneous tumor immunity, (ii) tumor immunity induced by PD-L1-checkpoint blockade, (iii) and adoptive TAA-specific T-cell-transfusion-mediated tumor immunity. In the first model, we treated mice carrying MC38 cancer cells with apoptotic T_{reg} cells. We found that tumor volumes were larger in mice that received apoptotic T_{reg} cells compared with those in control mice (Fig. 2e). Then, we examined the potential effect of apoptotic T_{reg} cells on anti-PD-L1 therapy in this model. PD-L1 blockade reduced tumor growth (Fig. 2e) and enhanced the expression of effector T cell cytokines in tumor-draining lymph nodes (Fig. 2f) and tumor tissue (Fig. 2g). However, apoptotic T_{reg} cells abolished these antitumor effects mediated by anti-PD-L1 (Fig. 2e–g). Thus, apoptotic T_{reg} cells inhibit spontaneous and checkpoint-blockade-induced antitumor immunity.

Finally, we explored the role of apoptotic T_{reg} cells in two adoptive TAA-specific T cell transfer models. We transfused MHC class I–restricted (ovalbumin (OVA)-specific; OT-I) T cell receptor–transgenic T cells into ID8-OVA-bearing (otherwise wild-type) mice and then treated the mice with apoptotic T_{reg} cells and live T_{reg} cells. Both apoptotic T_{reg} cells and live T_{reg} cells promoted tumor growth (Supplementary Fig. 2d) and inhibited effector T cell cytokine expression (Supplementary Fig. 2e,f). However, apoptotic T_{reg} cells demonstrated superior suppressor activity compared with that of live T_{reg} cells (Supplementary Fig. 2d–f). In addition, we transferred T cell receptor–transgenic $CD8^+$ T cells that specifically recognized the melanoma antigen PMEL into B16-F10-bearing *Rag2*$^{-/-}$ mice. We treated the mice with apoptotic T_{reg} cells and anti-PD-L1 mAb (Supplementary Fig. 2g). Again, we found that apoptotic T_{reg} cells suppressed PMEL-specific T cell immunity and disabled the antitumor effect of PD-L1 blockade, as shown by increased tumor growth (Fig. 2h), shortened mouse survival (Fig. 2i), and reduced numbers of IFN-γ^+TNF$^+$ polyfunctional effector T cells (Fig. 2j,k). Thus, apoptotic T_{reg} cells were superior suppressors in multiple *in vitro* and *in vivo* models.

Apoptotic T_{reg} cells make suppressive nonprotein factor(s)

Next, we studied the cellular and molecular mechanisms by which apoptotic T_{reg} cells suppress T cell activation. Myeloid cells, including macrophages, can process apoptotic cells and may mediate immunosuppression in the tumor microenvironment[28,29]. To explore whether apoptotic T_{reg} cell–mediated immunosuppression depends on macrophages, we tested the effect of apoptotic T_{reg} cells on tumor immune response with macrophage

depletion in an MC38 model. As expected, the addition of apoptotic T_{reg} cells and the depletion of macrophages promoted and inhibited tumor growth, respectively (Fig. 3a). Accordingly, polyfunctional effector T cell cytokine expression was suppressed after the addition of apoptotic T_{reg} cells and enhanced after macrophage depletion (Fig. 3b,c). Apoptotic T_{reg} cells remained immunosuppressive after macrophage depletion (Fig. 3a–c). These observations suggest that macrophages are dispensable for apoptotic T_{reg} cell–mediated immunosuppression in this system.

On the molecular level, live T_{reg} cells express Foxp3 and can mediate immunosuppression via multiple modes of action[5,30,31]. Immunoblotting showed high levels of immunosuppression-associated membrane molecules, including PD-L1, PD-1, CTLA-4, CD39, and CD73, in apoptotic T_{reg} cells compared with the amounts in conventional T cells, regardless of their live status (Fig. 3d). PD-1 and PD-L1 blockade with specific antibodies had no effect on the suppressive properties of apoptotic T_{reg} cells (Fig. 3e). Apoptotic T_{reg} cells from PD-L1-deficient (*Cd274*$^{-/-}$) (Fig. 3f), PD-1-deficient (*Pdcd1*$^{-/-}$) (Fig. 3g), and wild-type mice suppressed T cell IL-2 expression to similar degrees (Fig. 3f,g). CTLA-4 blockade did not change the suppressive activity of apoptotic T_{reg} cells (Supplementary Fig. 3a–c). In addition to membrane proteins, it is possible that, similarly to live T_{reg} cells, apoptotic T_{reg} cells may release soluble factors including cytokines to mediate T cell suppression. To test this possibility, we collected apoptotic T_{reg} cell–derived supernatants via ultracentrifugation. The supernatants from apoptotic T_{reg} cells inhibited T cell IL-2 expression in a dose-dependent manner (Supplementary Fig. 3d). However, neutralization of the immunosuppressive cytokine TGF-β (Supplementary Fig. 3e–g), IL-35 subunit EBI3 (Supplementary Fig. 3h–j), and IL-10 (Supplementary Fig. 3k–m) with blocking antibodies did not rescue this suppression. Thus, apoptotic T_{reg} cells release unknown soluble immunosuppressive factor(s), and TGF-β, IL-35, and IL-10 are not involved in apoptotic T_{reg} cell–mediated T cell suppression.

To identify the soluble suppressive factor(s), we divided the apoptotic T_{reg} cell supernatants into two fractions with a 3-kDa molecular-weight-cutoff filter. We observed that the fraction above 3 kDa did not suppress T cell IL-2 production, whereas the fraction below 3 kDa did (Fig. 3h). This molecular weight is consistent with the observations that PD-L1, PD-1, CTLA-4, IL-10, TGF-β, and IL-35 were not involved in the suppressive function of apoptotic T_{reg} cells (Fig. 3e–g and Supplementary Fig. 3). Supernatants from apoptotic T_{reg} cells remained immunosuppressive after treatment with proteinase K (Fig. 3i) or trypsin (Fig. 3j). However, incubation with dextran-coated charcoal resulted in a loss of immunosuppression (Fig. 3k). The data suggest that the soluble immunosuppressive factors may be small molecules, rather than proteins or large peptides.

Apoptotic T_{reg} cells mediate suppression via the A_{2A} pathway

We attempted to define the molecular nature of apoptotic T_{reg} cell–derived suppressive supernatants. Live mouse T_{reg} cells express CD39 and CD73 and can convert ATP to adenosine[32]. Live human cancer-infiltrating T_{reg} cells express CD39 and CD73 and inhibit effector T cells through an adenosinergic pathway[33]. We noticed that mouse apoptotic T_{reg} cells expressed CD39 and CD73 (Fig. 3d) and released a nonprotein small

immunosuppressive molecule (or molecules) (Fig. 3h–k and Supplementary Fig. 3). Thus, we hypothesized that CD39 and CD73 in apoptotic T_{reg} cells remain enzymatically active and could mediate adenosine production, and that the nonprotein small immunosuppressive molecule might be adenosine. To test this hypothesis, we induced apoptosis in mouse T_{reg} cells with anti-Fas mAb and kinetically measured adenosine in the supernatants. A colorimetric assay detected high amounts of adenosine at 6 h in the apoptotic T_{reg} cell supernatants, but not in live T_{reg} cell medium (Fig. 4a). Mass spectrometry (Supplementary Fig. 4a,b) detected a kinetic increase in adenosine levels in apoptotic T_{reg} cell supernatants (Supplementary Fig. 4b,c). The amounts of adenosine also peaked at hour 6 of T_{reg} cell apoptosis (Supplementary Fig. 4c). Then, we examined the potential suppressive role of adenosine in apoptotic T_{reg} cell supernatants. The addition of exogenous adenosine to mouse T cell cultures led to reduced production of TNF and IL-2 (Fig. 4b,c). A_{2A} is a receptor for adenosine in T cells[34] and mediates IL-2 suppression in particular[35]. We observed that the A_{2A} inhibitor ZM241385 abolished T cell effector cytokine suppression mediated by apoptotic T_{reg} cell supernatants (Fig. 4d,e). We extended these mouse studies to human ovarian cancer. Again, the supernatants of human ovarian-cancer-infiltrating apoptotic T_{reg} cells inhibited T cell activation. The effect was abrogated by ZM241385 (Fig. 4f,g). Thus, apoptotic T_{reg} cells mediate immunosuppression via adenosine and the A_{2A} pathway.

Apoptotic T_{reg} cells release ATP and metabolize it to adenosine

Next, we explored how apoptotic T_{reg} cells produce a large amount of adenosine in the absence of exogenous ATP. Gene set enrichment analysis demonstrated that mouse B16-melanoma-infiltrating T_{reg} cells showed active expression of genes associated with purine and pyrimidine metabolism (GSE55705)[26] (Supplementary Fig. 5a,b), suggesting high energy metabolism. We hypothesized that apoptotic T_{reg} cells generate, release, and consequently metabolize to adenosine high levels of ATP via apoptotic-cell-associated CD39 and CD73, and ultimately suppress T cell activation via adenosine in the tumor. To test this hypothesis, we induced apoptosis in mouse T_{reg} cells and conventional T cells by anti-Fas treatment (Fig. 5a), serum starvation (Fig. 5b), or irradiation (Fig. 5c). After the induction of apoptosis, T_{reg} cells, but not conventional T cells, released a large amount of ATP (Fig. 5a,b), possibly owing to the higher ATP content in T_{reg} cells (Supplementary Fig. 5c). Apoptotic cells can release small molecules via pannexin-1-dependent channels[36]. We found that treatment with pannexin-1 inhibitor (probenecid or carbenoxolone) prevented apoptotic T_{reg} cells from releasing ATP into supernatants (Supplementary Fig. 5d). Thus, apoptotic T_{reg} cells release ATP via pannexin-1-dependent channels.

The amount of ATP released from apoptotic T_{reg} cells peaked between 0.5 and 2 h and decreased to baseline at 6–8 h after apoptosis (Fig. 5a). This suggests that ATP may be metabolized and converted into adenosine. In line with this, the measured amounts of adenosine inversely correlated with those of ATP and peaked at 6 h after apoptosis in supernatants from apoptotic T_{reg} cells (Fig. 5d). To determine the ability of apoptotic T_{reg} cells to generate adenosine, we incubated apoptotic T_{reg} cells in medium containing exogenous ADP or ATP. We detected higher amounts of adenosine in culture medium containing apoptotic T_{reg} cells than in the control samples (Fig. 5e). We collected the supernatants from these experiments and filtered them with a 3-kDa-cutoff filter. Again,

these supernatants mediated potent suppression in T cell cytokines (Fig. 5f). The data suggest that apoptotic T_{reg} cells can convert ADP and ATP to adenosine.

Apoptotic T_{reg} cells express CD39 and CD73 (Fig. 3d). To directly determine whether CD39 and CD73 are functional in apoptotic T_{reg} cells, we treated apoptotic T_{reg} cells with a CD39 inhibitor, ARL67156, and a CD73 inhibitor, AMP-CP. As expected, ARL67156, but not AMP-CP, prevented ATP degradation (Fig. 5g). Furthermore, CD39 and CD73 inhibitors rescued IL-2 expression that was inhibited by apoptotic T_{reg} cells (Fig. 5h). To genetically validate our observation, we tested the suppressive activity of apoptotic T_{reg} cells from CD73-deficient (*Nt5e*$^{-/-}$) mice. Live *Nt5e*$^{-/-}$ and wild-type T_{reg} cells contained similar amounts of intracellular ATP (Supplementary Fig. 5e). *Nt5e*$^{-/-}$ and wild-type apoptotic T_{reg} cells released similar amounts of ATP into the medium (Supplementary Fig. 5f). However, *Nt5e*$^{-/-}$ apoptotic T_{reg} cells generated less adenosine (Supplementary Fig. 5g) and were less immunosuppressive than wild-type apoptotic T_{reg} cells (Fig. 5i,j). Next, we treated MC38-tumor-bearing mice with apoptotic *Nt5e*$^{-/-}$ T cells and apoptotic wild-type T_{reg} cells. We found that tumor volumes were larger in mice that received apoptotic wild-type T_{reg} cells than in those administered apoptotic *Nt5e*$^{-/-}$ T_{reg} cells (Fig. 5k), which indicated that apoptotic *Nt5e*$^{-/-}$ T_{reg} cells were less suppressive than apoptotic *Nt5e*$^{+/+}$ T_{reg} cells. In addition, we tested whether ARL67156 (Fig. 5l) and ZM241385 (Fig. 5m) affect apoptotic T_{reg} cell–mediated immunosuppression in MC38-tumor-bearing mice with or without PD-L1 blockade. As shown by changes in tumor volume, the two inhibitors partially subverted the immunosuppressive effect of apoptotic T_{reg} cells and additionally improved the therapeutic outcome of PD-L1 blockade (Fig. 5l,m). Together, our data suggest that apoptotic T_{reg} cells release high levels of ATP and metabolize it to adenosine via the CD39 and CD73 axis, and suppress T cells through interaction with adenosine and A_{2A} receptors.

Oxidative stress induces T_{reg} cell apoptosis in tumors

Finally, we explored why T_{reg} cells undergo apoptosis in the tumor microenvironment. Effector T cells are affected by glycolytic metabolism in the tumor microenvironment[13,14,16]. To explore whether tumor T_{reg} cell apoptosis can be attributed to poor glycolysis, we treated normal T_{reg} cells and conventional T cells with or without glucose and the hexokinase inhibitor 2-deoxy-D-glucose. Glucose restriction and 2-deoxy-D-glucose treatment induced apoptosis in conventional T cells (Supplementary Fig. 6a), but not in T_{reg} cells (Supplementary Fig. 6b). Oxidative stress disrupts DC function in ovarian cancer[25]. Thus, we tested whether oxidative stress induces T_{reg} cell apoptosis via reactive oxygen species (ROS) in the tumor microenvironment. To this end, we treated human T_{reg} cells with ovarian cancer ascites. We found that treatment with ovarian cancer ascites and hydrogen peroxide (H_2O_2) induced potent apoptosis in T_{reg} cells, but not in conventional T cells (Fig. 6a and Supplementary Fig. 6c). T_{reg} cell apoptosis was reversed by treatment with the ROS scavenger *N*-acetyl-cysteine (Fig. 6a). Ovarian cancer ascites (Fig. 6b,c) and H_2O_2 treatment (Fig. 6d,e) led to higher expression of proapoptotic genes (Fig. 6b,d) and lower expression of antiapoptotic genes (Fig. 6c,e) in T_{reg} cells compared with controls. Furthermore, we detected high concentrations of the major ROS component superoxide in ovarian cancer ascites (Supplementary Fig. 6d). Ovarian-cancer-infiltrating T_{reg} cells showed high mitochondrial activity compared with that in conventional T cells

(Supplementary Fig. 6e) and produced higher amounts of intracellular ROS (Supplementary Fig. 6f). Thus, T_{reg} cells are relatively more sensitive to oxidative stress in the tumor microenvironment than conventional T cells are, and undergo potent apoptosis.

Next, we wondered why T_{reg} cells are more vulnerable to oxidative stress. The cellular antioxidant system is largely regulated by the transcription factor NRF2 (*Nfe2l2*) and its associated genes[37,38]. We quantified the expression of *Nfe2l2* and NRF2-associated gene transcripts including *Gclm*, *Gclc*, *Hmox1*, *Nqo1*, and *Ggct* in normal T_{reg} cells and conventional T cells. The levels of the majority of these antioxidant gene transcripts were lower in mouse (Fig. 6f) and human (Supplementary Fig. 6g) T_{reg} cells than in conventional T cells. Immunoblotting showed lower amounts of NRF2, GLCM, and heme oxygenase (HO-1) proteins in mouse (Fig. 6g) and human (Supplementary Fig. 6h) T_{reg} cells than in conventional T cells. Concentrations of intracellular ROS were higher in T_{reg} cells than in conventional T cells (Fig. 6h). Next, we tested the influence of the NRF2 inducers diethylmaleate and sulforaphane on T_{reg} cell apoptosis in the presence of ovarian cancer ascites. Both NRF2 inducers reduced T_{reg} cell apoptosis compared with that in the control (Fig. 6i). Furthermore, we treated MC38-tumor-bearing mice with sulforaphane. We found that treatment with sulforaphane reduced T_{reg} cell apoptosis (Fig. 6j), increased effector T cell cytokine expression (Fig. 6k), and inhibited tumor growth (Fig. 6l) compared with that observed in the control. Taken together, these data indicate that oxidative stress results in apoptosis of T_{reg} cells via ROS in the tumor microenvironment, which in turn increases their suppressive action.

DISCUSSION

T_{reg} cells are recruited into the tumor microenvironment. It is thought that live, but not apoptotic, T_{reg} cells mediate immune suppression[1,2,4–6]. In this work, we studied T_{reg} cells in human ovarian cancer and in several mouse tumors. We found that T_{reg} cells underwent potent apoptosis in human and mouse tumor microenvironments. To our surprise, apoptotic T_{reg} cells were more efficient than live T_{reg} cells at suppressing T cell activation *in vitro* and *in vivo*. More important, we demonstrated that the therapeutic efficacy of PD-L1 blockade was abolished by apoptotic T_{reg} cells in tumor-bearing mouse models. The majority of cancer patients remain unresponsive to therapies based on PD-L1 and PD-1 signaling blockade[39], and we wondered whether this clinical unresponsiveness (or therapeutic resistance) is associated with high degrees of T_{reg} cell apoptosis in the tumor microenvironment. Furthermore, the targeting of T_{reg} cells is considered a potential therapeutic strategy for cancer treatment. However, clinical trials with T_{reg} cell depletion have not been translated into therapeutic efficacy in people with cancer[40–43]. This raises the possibility that therapeutic induction of T_{reg} cell apoptosis may sustain and/or amplify, rather than disable, T_{reg}-cell-mediated immunosuppression.

PD-L1, CTLA-4, TGF-β, IL-10, and IL-35 are well-defined immunosuppressive components for live T_{reg} cells[1–6]. Our biochemical analysis and *in vivo* functional studies demonstrated that these molecules are not involved in the suppressor activity of apoptotic T_{reg} cells. Live T_{reg} cells express the ectoenzymes CD39 and CD73 and can convert extracellular ATP to adenosine, and in turn mediate immunosuppression via adenosine and

the A_{2A} receptor signaling pathway[32]. We observed that apoptotic T_{reg} cells release a large amount of ATP and efficiently convert ATP into immunosuppressive adenosine via CD39 and CD73 *in vitro* and *in vivo*. Therefore, it can be assumed that CD39 and CD73 remain enzymatically active in apoptotic T_{reg} cells. Furthermore, apoptotic T_{reg} cells released a large amount of ATP into the extracellular space via pannexin-1 channels. In line with our observation, mouse apoptotic thymocytes release low-molecular-mass compounds via pannexin-1 channels[36]. Thus, apoptotic T_{reg} cells can self-supply and release ATP, and convert it to adenosine in the local environment. We propose a novel immune-evasion mechanism: tumor-infiltrating T_{reg} cells inadvertently die to mediate, sustain, and amplify powerful suppression in the tumor microenvironment.

It has been reported that Foxp3 is a proapoptotic factor for T_{reg} cells in mouse thymus, unless some surviving factors such as γ-chain cytokines are present[44]. We have explored the potential molecular mechanism of T_{reg} cell apoptosis in the tumor microenvironment. Several metabolic checkpoint molecules, including AMPK, mTORC1 (refs. [20,21]), and HIF-1α (refs. [22,23]), may physiologically regulate T_{reg} cell function and the balance between T_{reg} cells and effector T cells in mouse models. However, how T_{reg} cells (particularly human tumor T_{reg} cells) behave in the metabolically abnormal tumor microenvironment remains unknown. Glycolysis profoundly alters effector T cell phenotype and function in the tumor microenvironment[14–16]. We observed that T_{reg} cells were not as sensitive as effector memory T cells to glycolytic restriction. Instead, we found that T_{reg} cells were vulnerable to oxidative stress in the tumor microenvironment. Our data show that free oxygen species target mitochondria and induce apoptosis in T_{reg} cells, consequently triggering the suppressive cascade of T_{reg} cells in the tumor microenvironment. Thus, our current study complements recent reports on the metabolic control of memory T cells[14–16] and DCs[25] and extends to T_{reg} cells in human and mouse tumor microenvironments.

In summary, apoptotic T_{reg} cell–mediated immunosuppression may be a major mode of action for T_{reg} cells in cancer and serve as a potential mechanism for checkpoint-blockade resistance. Furthermore, T_{reg} cell apoptosis triggered by oxidative stress is a novel tumor immune-evasion mechanism in the tumor microenvironment, and targeting tumor metabolism is a potential therapeutic strategy for cancer treatment.

METHODS

Methods, including statements of data availability and any associated accession codes and references, are available in the online version of the paper.

ONLINE METHODS

Ovarian cancer patients, cancer tissues, ascites, and cells

People diagnosed with high-grade serous ovarian carcinomas were recruited for this study, and informed consent was obtained from all participants. The use of human subjects for this study was approved by the University of Michigan Institutional Review Board. We used clinical samples from people who had received no prior anticancer therapies. Fresh tumor tissues and tumor ascites were processed into single-cell suspensions for phenotype and

functional studies. Tumor ascites were centrifuged, and cell-free fractions were frozen at −80 °C.

Cell transfection

ID8 cells were transfected with plasmid pCI-neo-mOVA (Addgene plasmid #25099)[45]. Lipofectamine 2000 (Invitrogen) was used for delivery according to the vendor's instructions. The cells were selected with geneticin (Invitrogen), and ovalbumin expression was confirmed by flow cytometry and used for *in vivo* mouse experiments.

Animals

Animal experiments were approved by the University of Michigan Institutional Review Board. Wild-type female C57BL/6J, C57BL/6 Foxp3^{-}GFP^{+} (C57BL/6-Tg(Foxp3-GFP)90Pkraj/J), B6.SJL-*Ptprc*^{a}*Pepc*^{b}/BoyJ, C57BL/6-Tg(TcraTcrb)1100Mjb/J, B6.Cg-Thy1a/Cy Tg(TcraTcrb)8Rest/J, and *Nt5e*$^{-/-}$ C57BL/6 mice (8–10 weeks old) were obtained from the Jackson Laboratories. PD-L1-deficient (*Cd274*$^{-/-}$) and PD-1-deficient (*Pdcd1*$^{-/-}$) C57BL/6 mice were originally provided by Dr. Lieping Chen at Yale University and Dr. Tasuku Honjo at Kyoto University, respectively.

In vivo tumor experiments

For tumor growth experiments, the animals were inoculated intraperitoneally (i.p.) with 1.5 × 10^6 ID8 ovarian cancer cells, or subcutaneously with 10^6 MC38 cells or 3 × 10^5 B16-F10 cells. When tumor cells were coinjected with apoptotic or live T cells, the ratio was 1:1.

For the PMEL-specific mouse model, T cell transfer was accomplished by a single intravenous injection of 10^6 PMEL-specific CD8^{+} T cells. Donor CD8^{+} T cells were collected from spleens and lymph nodes of B6.Cg-Thy1a/Cy Tg(TcraTcrb)8Rest/J mice and expanded with plate-bound anti-CD3 and soluble anti-CD28 in the presence of recombinant mouse IL-2. Expanded T cells were transferred to mice bearing B16-F10 tumors. Animals were treated as described in Supplementary Figure 2g.

For the OVA-specific model, ID8-OVA-Luc tumor cells were inoculated into B6.SJL-*Ptprc*^{a}*Pepc*^{b}/BoyJ mice, which are congenic B6 animals that express CD45.1 antigen. After 7 d, the mice received 10^6 OVA-specific CD45.2^{+}CD8^{+} T cells i.p. Animals were treated as described in Supplementary Figure 2d–f. 10 min after the injection of 150 mg/kg body mass D-luciferin (Promega), the bioluminescence of luciferase-expressing tumors was assessed with the IVIS 200 Spectrum imaging system (PerkinElmer).

Treatments with anti-PD-L1 or isotype control antibody (both from Bio X Cell) were done between days 7 and 20 (20 mg/kg i.p.).

Macrophages were depleted with clodronate liposome (Liposoma). Liposomes containing clodronate or control liposomes were injected into mice on days 4, 6, 8, and 10 (200 μl i.p.).

All tumor cell lines used in the experiments were routinely tested for mycoplasma contamination by PCR assay. Randomization of animals was not used in experiments. No blinding was done.

Cell culture and biochemical reagents

RPMI 1640 medium supplemented with 10% FBS (Invitrogen) was used for the majority of the experiments. For cultures without glucose, the cells were treated with RPMI 1640 medium without glucose (Sigma-Aldrich) and charcoal-treated FBS (Invitrogen). Probenecid, carbenoxolone, diethylmaleate, L-sulforaphane, *N*-acetyl-cysteine, H_2O_2, ZM241385, AMP-CP, ARL67165, EHNA, ADP, ATP, and adenosine were obtained from Sigma-Aldrich. Cell lines were obtained from the US National Institutes of Health or ATCC. All cell lines were routinely tested for mycoplasma contamination.

Isolation and culture of T_{reg} cells and conventional T cells

Single-cell suspensions were prepared from mouse and human tissues including tumor tissues, tumor ascites, and tumor-draining lymph nodes as previously reported[46–49]. Mouse $Foxp3^+GFP^+$ T_{reg} cells were enriched and sorted from spleen and lymph nodes and/or were generated in the presence of IL-2 (10 ng/ml) and TGF-β (10 ng/ml). Human T cells were isolated from healthy donor buffy coats (Carter BloodCare) and purified directly with RosetteSep human T cell enrichment kits (StemCell Technologies). T_{reg} cells from human tumors were isolated with a commercially available T_{reg} cell isolation kit (StemCell) and confirmed by Foxp3 staining.

Induction of T_{reg} cell apoptosis

T_{reg} cells and conventional T cells (5×10^6 cells/ml) were incubated with anti-Fas mAb (10 μg/ml; clone Jo-1; eBioscience) for 15–30 min, washed, and suspended for further experiments. Apoptotic T_{reg} cells were also induced by 70-Gy irradiation and cultured serum-free for 24 h and with 5-fluorouracil for 24 h as indicated. For adenosine measurement, erythro-9-(2-hydroxy-3-nonyl) adenine (EHNA), an inhibitor of adenosine deaminase, was used to prevent adenosine degradation over time.

Apoptotic T_{reg} cell–derived supernatants

Apoptotic T_{reg} cell suspensions were centrifuged at 500*g* for 5 min, 18,000*g* for 1 h, and 12,000*g* overnight.

Immunosuppression assay

$CD4^+Foxp3^-$ responder T cells were cocultured with live T_{reg} cells or apoptotic T_{reg} cells or with apoptotic T_{reg} cell–derived supernatants in 96-well round-bottom plates at a ratio of 1:2 in the presence of anti-CD3 (2.5 μg/mL) and irradiated antigen-presenting cells. In some experiments, anti-PD-L1 (eBioscience), anti-PD-1 (eBioscience), anti-TGF-β (R&D), anti-CTLA-4 (BD), anti-IL-10 (eBioscience), and anti-EBI3 (Millipore) blocking antibodies were added into the culture at a final concentration of 10 μg/ml. Cells and culture supernatants were collected for cytokine quantification by flow cytometry analysis and ELISA.

Depletion of proteins and small molecules from T_{reg} cell supernatants

To remove proteins from apoptotic or control T_{reg} cell supernatants, we applied proteinase K or trypsin treatment for 1 h at 37 °C. Next, we inactivated enzymes by boiling samples for 5

min and removed precipitates by centrifugation at 10,000*g* for 10 min at 4 °C. For the removal of small molecules including lipids, hormones, and nucleotides, media were treated with dextran-coated charcoal (DCC). Briefly, 0.5% (m/v) DCC suspension was mixed with the supernatants at a volume ratio of 5:1 and incubated at room temperature for 20 min. Next, DCC was removed by centrifugation at 7,000*g*, 30 min, 4 °C. The supernatants were collected for further experiments.

Small-molecule assays

For the ATP assay, pellets of T_{reg} cells and conventional T cells were directly suspended in 1 M perchloric acid and used for ATP assays or stored at −80 °C for further testing. Media were deproteinized with 4 M perchloric acid for further use. A colorimetric ATP measurement kit (Pierce) was used according to the manufacturer's instructions. To measure adenosine, we used adenosine deaminase (Sigma Aldrich) to transform adenosine to xanthine in $HClO_4$-deproteinized media, and then we measured xanthine by colorimetric assay (BioVision).

Adenosine was also detected by liquid chromatography coupled with tandem mass spectrometry. Cell culture medium was collected and analyzed freshly in an LC–triple quadrupole mass spectrometer (Agilent 6490 series) with a jet stream electrospray ionization source (Agilent). Chromatography was carried out on a Phenomenex Luna NH2 column (1 × 150 mm) and Agilent 1290 series liquid chromatograph. Mobile phase A was 5 mM ammonium acetate in LC-MS-grade water, pH adjusted to 9.9 with ammonium hydroxide. Mobile phase B was acetonitrile. 200 μl of extraction solvent was added to 200 μl of medium and vertexed briefly. A series of calibration standards (adenosine: 0, 0.01, 0.03, 0.1, 0.3, 1, and 5 μg/ml) were prepared along with the samples. The following transitions were used to identify and quantify adenosine: m/z 266.1 → m/z 134.1. Data were processed by MassHunter workstation software, version B.06. Experiments were performed with biological replicates. Each data point was acquired from cells harvested from different animals.

ELISA

T cell culture supernatants were collected at the time points indicated in the relevant figures. T cell effector cytokines were detected with ELISA kits (R&D).

Real-time PCR

Total RNA was isolated from Trizol-lysed (Invitrogen) samples according to the manufacturer's instructions. A reverse-transcriptase reaction was performed with oligo-dT primers and AMV polymerase (Invitrogen). Real-time PCR reactions were carried out with the Fast-SYBR kit (Applied Biosystems) and the primers listed in Supplementary Table 3.

Flow cytometry

Antibodies were from BD Biosciences, eBioscience, or Invitrogen. For human cells, we used anti-CD45 (clone HI30), anti-CD3 (SK7), anti-CD4 (RPA-T4), anti-cCASP3 (9H19L2), anti-Foxp3 (PCH101), anti-TNF (MAb11), anti-IL-2 (MQ1-17H12), and anti-IFN-γ (4S.B3). Mouse cells were stained with anti-CD45 (30-F11), anti-CD45.1 (A20), anti-

CD45.2 (104), anti-CD3 (500A2), anti-CD4 (RM4-5), anti-CD8 (53-6.7), anti-cCASP3 (9H19L2), anti-Foxp3 (FJK-16s), anti-TNF (MP6-XT22), anti-IL-2 (JES6-5H4), and anti-IFN-γ (XMG1.2). For surface staining, the cells were incubated with antibodies for 20 min, washed, and fixed in Fix/Perm solution (BD Biosciences). After being washed with Perm/Wash buffer (BD Biosciences), the cells were stained intracellularly for 30 min, washed, and fixed in 4% formaldehyde (Sigma Aldrich). In the case of apoptosis detection in cell culture, the cells were stained with human recombinant annexin V (BD Biosciences) followed by 7-ADD. In the case of tissue samples, the cells were stained for viability with blue fluorescent fixable dye (Life Technologies) followed by annexin V and Foxp3. All samples were read on an LSR II cytometer (BD) and analyzed with FACS DIVA software v. 8.0 (BD Biosciences).

Immunofluorescence staining

Tumor tissues were fixed in 10% formalin and embedded in paraffin for immunofluorescence staining. Multiplexed fluorescence staining was done with the OpalTM 4-plex staining system (PerkinElmer). Tissue sections were stained with anti-CD3 (clone PS1, mouse IgG2a; Novocastra/Leica), anti–cleaved caspase-3 (rabbit polyclonal IgG; Cell Signaling), and anti-Foxp3 (clone 259D, mouse IgG1; BioLegend). The secondary antibodies used were goat anti-mouse IgG2-α conjugated with Alexa Fluor 488 or goat anti-rabbit IgG (H+L) conjugated with Alexa Fluor 568. Staining slides were analyzed with the Mantra Quantitative Pathology Workstation (PerkinElmer).

Immunoblotting

After centrifugation cells were dissolved in cell lysis buffer (50 mm Tris-HCl, pH 7.4, 1% Triton X-100, 0.2% sodium deoxycholate, 0.2% SDS, 1 mM sodium EDTA) supplemented with protease inhibitors (5 μg/ml leupeptin, 5 μg/ml aprotinin, and 1 mM phenylmethylsulfonyl fluoride) and protein concentrations were determined with Bio-Rad protein assay reagent. The lysates were boiled for 5 min in Laemmli sample buffer (50 mm Tris-HCl, pH 6.8, 12.5% glycerol, 1% SDS, 0.01% bromophenol blue, 5% 2-mercaptoethanol). Then they were analyzed by SDS–PAGE followed by western blotting with primary antibodies as follows: anti-human/mouse NRF2 (clone 1808Y; Abcam), anti-human/mouse GCLM (rabbit polyclonal; Abcam), anti-mouse/human PD1 (clone 7A11B1; Thermo Fisher Scientific), anti-mouse PD-L1 (goat polyclonal; R&D Systems), anti-mouse CTLA-4 (clone 63828; R&D Systems), anti-mouse CD39 (clone 495826; R&D Systems), and anti-mouse CD73 (clone sc-32299; Santa Cruz Biotechnology). Proper secondary HRP-conjugated anti-rat, anti-rabbit (both from Vector Laboratories), or anti-goat (Santa Cruz Biotechnology) antibodies were used as secondary reagents.

Bioinformatics

Publicly available microarray data were analyzed with GSEA software v. 2.0, which is freely available from the Broad Institute (http://www.broad.mit.edu/gsea/)[50].

Statistics

Statistical analysis was done with R v. 3.0.2. For comparison of two groups, we used two-sided Student's *t*-test or Mann–Whitney *U*-test, depending on the data distribution (Shapiro–

Wilk test) and homogeneity of variance (Fisher's test or Levene's test). Parametrical or nonparametrical ANOVA tests accompanied by two-sided *post hoc* analysis were used for multiple-comparison experiments.

Data availability

A **Life Sciences Reporting Summary** for this paper is available.

Supplementary Material

Refer to Web version on PubMed Central for supplementary material.

Acknowledgments

This work was supported (in part) by the US National Institutes of Health (grants CA217540, CA123088, CA099985, CA156685, CA171306, CA190176, CA193136, CA211016, and 5P30CA46592 to W.Z.), the Ovarian Cancer Research Fund, and the Marsha Rivkin Center for Ovarian Cancer Research (W.Z.; I.K.). We are grateful to L. Carter and X. Hu for critical discussions about the A_{2A} pathway. We thank D. Postiff, M. Vinco, R. Craig, and J. Barikdar at the Tissue and Molecular Pathology Core for their assistance. We thank C. Ruan and S. Bridges at the Metabolomics Core for their support. *Cd274*−/− mice and *Pdcd1*−/− mice were provided by L. Chen (Yale University, New Haven, Connecticut, USA) and T. Honjo (Kyoto University, Kyoto, Japan), respectively.

References

1. Hori S, Nomura T, Sakaguchi S. Control of regulatory T cell development by the transcription factor Foxp3. Science. 2003; 299:1057–1061. [PubMed: 12522256]
2. Fontenot JD, Gavin MA, Rudensky AY. Foxp3 programs the development and function of $CD4^+CD25^+$ regulatory T cells. Nat Immunol. 2003; 4:330–336. [PubMed: 12612578]
3. Chen W, et al. Conversion of peripheral $CD4^+CD25^-$ naive T cells to $CD4^+CD25^+$ regulatory T cells by TGF-β induction of transcription factor Foxp3. J Exp Med. 2003; 198:1875–1886. [PubMed: 14676299]
4. Curiel TJ, et al. Specific recruitment of regulatory T cells in ovarian carcinoma fosters immune privilege and predicts reduced survival. Nat Med. 2004; 10:942–949. [PubMed: 15322536]
5. Sakaguchi S. Naturally arising Foxp3-expressing $CD25^+CD4^+$ regulatory T cells in immunological tolerance to self and non-self. Nat Immunol. 2005; 6:345–352. [PubMed: 15785760]
6. Zou W. Regulatory T cells, tumour immunity and immunotherapy. Nat Rev Immunol. 2006; 6:295–307. [PubMed: 16557261]
7. Li MO, Sanjabi S, Flavell RA. Transforming growth factor-β controls development, homeostasis, and tolerance of T cells by regulatory T cell-dependent and -independent mechanisms. Immunity. 2006; 25:455–471. [PubMed: 16973386]
8. Liu Y, et al. A critical function for TGF-β signaling in the development of natural $CD4^+CD25^+Foxp3^+$ regulatory T cells. Nat Immunol. 2008; 9:632–640. [PubMed: 18438410]
9. Maruyama T, et al. Control of the differentiation of regulatory T cells and T_H17 cells by the DNA-binding inhibitor Id3. Nat Immunol. 2011; 12:86–95. [PubMed: 21131965]
10. Ouyang W, et al. Novel Foxo1-dependent transcriptional programs control T_{reg} cell function. Nature. 2012; 491:554–559. [PubMed: 23135404]
11. Vander Heiden MG, Cantley LC, Thompson CB. Understanding the Warburg effect: the metabolic requirements of cell proliferation. Science. 2009; 324:1029–1033. [PubMed: 19460998]
12. Gubser PM, et al. Rapid effector function of memory $CD8^+$ T cells requires an immediate-early glycolytic switch. Nat Immunol. 2013; 14:1064–1072. [PubMed: 23955661]
13. Chang CH, et al. Posttranscriptional control of T cell effector function by aerobic glycolysis. Cell. 2013; 153:1239–1251. [PubMed: 23746840]
14. Chang CH, et al. Metabolic competition in the tumor microenvironment is a driver of cancer progression. Cell. 2015; 162:1229–1241. [PubMed: 26321679]

15. Ho PC, et al. Phosphoenolpyruvate is a metabolic checkpoint of anti-tumor T cell responses. Cell. 2015; 162:1217–1228. [PubMed: 26321681]
16. Zhao E, et al. Cancer mediates effector T cell dysfunction by targeting microRNAs and EZH2 via glycolysis restriction. Nat Immunol. 2016; 17:95–103. [PubMed: 26523864]
17. Clever D, et al. Oxygen sensing by T cells establishes an immunologically tolerant metastatic niche. Cell. 2016; 166:1117–1131. [PubMed: 27565342]
18. Eil R, et al. Ionic immune suppression within the tumour microenvironment limits T cell effector function. Nature. 2016; 537:539–543. [PubMed: 27626381]
19. Singer M, et al. A distinct gene module for dysfunction uncoupled from activation in tumor-infiltrating T cells. Cell. 2016; 166:1500–1511. [PubMed: 27610572]
20. Delgoffe GM, et al. The mTOR kinase differentially regulates effector and regulatory T cell lineage commitment. Immunity. 2009; 30:832–844. [PubMed: 19538929]
21. Zeng H, et al. mTORC1 couples immune signals and metabolic programming to establish T_{reg}-cell function. Nature. 2013; 499:485–490. [PubMed: 23812589]
22. Shi LZ, et al. HIF1α-dependent glycolytic pathway orchestrates a metabolic checkpoint for the differentiation of T_H17 and T_{reg} cells. J Exp Med. 2011; 208:1367–1376. [PubMed: 21708926]
23. Dang EV, et al. Control of T_H17/T_{reg} balance by hypoxia-inducible factor 1. Cell. 2011; 146:772–784. [PubMed: 21871655]
24. Saito T, et al. Two $FOXP3^+CD4^+$ T cell subpopulations distinctly control the prognosis of colorectal cancers. Nat Med. 2016; 22:679–684. [PubMed: 27111280]
25. Cubillos-Ruiz JR, et al. ER stress sensor XBP1 controls anti-tumor immunity by disrupting dendritic cell homeostasis. Cell. 2015; 161:1527–1538. [PubMed: 26073941]
26. Arvey A, et al. Inflammation-induced repression of chromatin bound by the transcription factor Foxp3 in regulatory T cells. Nat Immunol. 2014; 15:580–587. [PubMed: 24728351]
27. Ko K, et al. Treatment of advanced tumors with agonistic anti-GITR mAb and its effects on tumor-infiltrating $Foxp3^+CD25^+CD4^+$ regulatory T cells. J Exp Med. 2005; 202:885–891. [PubMed: 16186187]
28. Cui TX, et al. Myeloid-derived suppressor cells enhance stemness of cancer cells by inducing microRNA101 and suppressing the corepressor CtBP2. Immunity. 2013; 39:611–621. [PubMed: 24012420]
29. Wan S, et al. Tumor-associated macrophages produce interleukin 6 and signal via STAT3 to promote expansion of human hepatocellular carcinoma stem cells. Gastroenterology. 2014; 147:1393–1404. [PubMed: 25181692]
30. Shevach EM. $CD4^+CD25^+$ suppressor T cells: more questions than answers. Nat Rev Immunol. 2002; 2:389–400. [PubMed: 12093005]
31. Vignali DAA, Collison LW, Workman CJ. How regulatory T cells work. Nat Rev Immunol. 2008; 8:523–532. [PubMed: 18566595]
32. Deaglio S, et al. Adenosine generation catalyzed by CD39 and CD73 expressed on regulatory T cells mediates immune suppression. J Exp Med. 2007; 204:1257–1265. [PubMed: 17502665]
33. Kryczek I, et al. Phenotype, distribution, generation, and functional and clinical relevance of Th17 cells in the human tumor environments. Blood. 2009; 114:1141–1149. [PubMed: 19470694]
34. Huang S, Apasov S, Koshiba M, Sitkovsky M. Role of A2a extracellular adenosine receptor-mediated signaling in adenosine-mediated inhibition of T-cell activation and expansion. Blood. 1997; 90:1600–1610. [PubMed: 9269779]
35. Erdmann AA, et al. Activation of Th1 and Tc1 cell adenosine A2A receptors directly inhibits IL-2 secretion *in vitro* and IL-2-driven expansion *in vivo*. Blood. 2005; 105:4707–4714. [PubMed: 15746085]
36. Chekeni FB, et al. Pannexin 1 channels mediate 'find-me' signal release and membrane permeability during apoptosis. Nature. 2010; 467:863–867. [PubMed: 20944749]
37. Sporn MB, Liby KT. NRF2 and cancer: the good, the bad and the importance of context. Nat Rev Cancer. 2012; 12:564–571. [PubMed: 22810811]
38. DeBerardinis RJ, Chandel NS. Fundamentals of cancer metabolism. Sci Adv. 2016; 2:e1600200. [PubMed: 27386546]

39. Zou W, Wolchok JD, Chen L. PD-L1 (B7-H1) and PD-1 pathway blockade for cancer therapy: mechanisms, response biomarkers, and combinations. Sci Transl Med. 2016; 8:328rv4.
40. Barnett B, Kryczek I, Cheng P, Zou W, Curiel TJ. Regulatory T cells in ovarian cancer: biology and therapeutic potential. Am J Reprod Immunol. 2005; 54:369–377. [PubMed: 16305662]
41. Dannull J, et al. Enhancement of vaccine-mediated antitumor immunity in cancer patients after depletion of regulatory T cells. J Clin Invest. 2005; 115:3623–3633. [PubMed: 16308572]
42. Attia P, Maker AV, Haworth LR, Rogers-Freezer L, Rosenberg SA. Inability of a fusion protein of IL-2 and diphtheria toxin (denileukin diftitox, DAB389IL-2, Ontak) to eliminate regulatory T lymphocytes in patients with melanoma. J Immunother. 2005; 28:582–592. [PubMed: 16224276]
43. Kurose K, et al. Phase Ia study of FoxP3^{+} CD4 T_{reg} depletion by infusion of a humanized anti-CCR4 antibody, KW-0761, in cancer patients. Clin Cancer Res. 2015; 21:4327–4336. [PubMed: 26429981]
44. Tai X, et al. Foxp3 transcription factor is proapoptotic and lethal to developing regulatory T cells unless counterbalanced by cytokine survival signals. Immunity. 2013; 38:1116–1128. [PubMed: 23746651]
45. Yang J, et al. Kupfer-type immunological synapse characteristics do not predict anti-brain tumor cytolytic T-cell function *in vivo*. Proc Natl Acad Sci USA. 2010; 107:4716–4721. [PubMed: 20133734]
46. Wang W, et al. Effector T cells abrogate stroma-mediated chemoresistance in ovarian cancer. Cell. 2016; 165:1092–1105. [PubMed: 27133165]
47. Peng D, et al. Epigenetic silencing of TH1-type chemokines shapes tumour immunity and immunotherapy. Nature. 2015; 527:249–253. [PubMed: 26503055]
48. Curiel TJ, et al. Blockade of B7-H1 improves myeloid dendritic cell–mediated antitumor immunity. Nat Med. 2003; 9:562–567. [PubMed: 12704383]
49. Zou W, et al. Stromal-derived factor-1 in human tumors recruits and alters the function of plasmacytoid precursor dendritic cells. Nat Med. 2001; 7:1339–1346. [PubMed: 11726975]
50. Subramanian A, et al. Gene Set Enrichment Analysis: a knowledge-based approach for interpreting genome-wide expression profiles. Proc Natl Acad Sci USA. 2005; 102:15545–15550. [PubMed: 16199517]

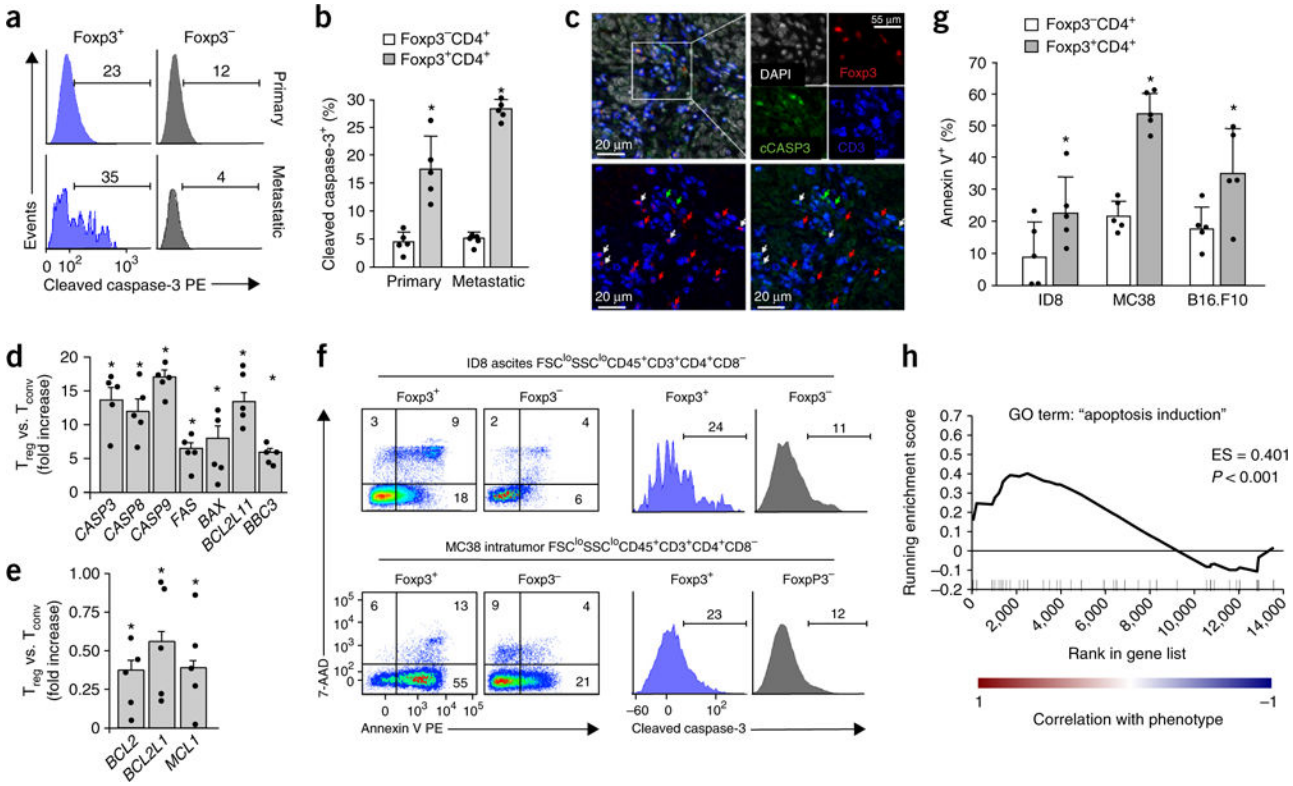

Figure 1.

T_{reg} cells are highly apoptotic in the tumor microenvironment. (**a,b**) Apoptotic Foxp3$^+$ T_{reg} cells and Foxp3$^-$ conventional T cells in human primary and metastatic ovarian cancers. Fresh human ovarian-cancer-infiltrating T cells were stained for viability, surface markers, Foxp3, and cleaved caspase-3. Polychromatic flow cytometry analysis was used to analyze cleaved caspase-3 expression in live CD45$^+$CD3$^+$CD4$^+$ cells. The representative histogram (**a**) and summarized data (**b**) show the relative amount of cleaved caspase-3$^+$ cells. Data in **b** are the mean and s.e.m. for $n = 5$ subjects. PE, phycoerythrin. (**c**) Cleaved caspase-3$^+$Foxp3$^+$ T_{reg} cells in human ovarian cancer tissues. Ovarian cancer tissue sections were stained for CD3 (blue), Foxp3 (red), cleaved caspase-3 (cCASP3; green), and nuclei (DAPI; white). The upper left image shows merged staining, and the white rectangle outlines the region of interest with high T cell infiltration. Single fluorescence channels for each antigen and DAPI are shown in the upper right. For detailed analysis (bottom), we overlaid the same region with the CD3 channel (blue) and the Foxp3 channel (red) (lower left) or with the CD3 channel (blue) and the cleaved caspase-3 channel (green) (lower right). The arrows indicate the same cells in both of the bottom images. Red arrows, Foxp3$^+$ cells; green arrows, cleaved caspase-3$^+$ cells; white arrows, triple-positive (Foxp3$^+$cCASP3$^+$CD3$^+$) cells. (**d,e**) The expression of proapoptotic (**d**) and antiapoptotic (**e**) genes in human ovarian-cancer-infiltrating T_{reg} cells. Results are shown as the fold change in expression of each gene in T_{reg} cells after normalization to expression in conventional T cells (T_{conv}) isolated from the same cancer tissue. Data shown are the mean and s.e.m. of $n = 5$ individual subjects. (**f,g**) Apoptotic T_{reg} cells and conventional T cells in mouse tumor tissues. We prepared single-cell suspensions from mouse ID8 ovarian cancer, MC38 colon cancer, and B16 melanoma

and stained the cells for annexin V, 7-AAD, and cleaved caspase-3. The representative plots in **f** show the percentages of apoptotic cells in $Foxp3^{+}CD4^{+}$ and $Foxp3^{-}CD4^{+}$ T cells as assessed on the basis of annexin V or cleaved caspase-3 expression. Numbers in corners indicate the percentage of cells in the gate. The results shown in **g** are the mean percentages ($^{+}$ s.e.m.) of annexin V^{+} cells among all cells in the group; $n = 5$ mice. (**h**) Gene set enrichment analysis of apoptosis genes in tumor-associated T_{reg} cells versus conventional T cells from the GSE55705 data set. The enrichment score (ES) and *P* value are reported for the GO term "apoptosis induction" and were calculated by GSEA with weighted enrichment statistics and ratio of classes for the metric as input parameters. Images and data are pooled from 5 experiments (**b,d,e**) or from 1 experiment with 5 animals (**g**) or are representative of single experiments with 5 subjects (**a,f**), 10 subjects (**c**), or 2 subjects per group (**h**). $*P < 0.05$, Wilcoxon test (**b**) or Student's *t*-test (**g**); $*P < 0.01$, Wilcoxon test (**d,e**).

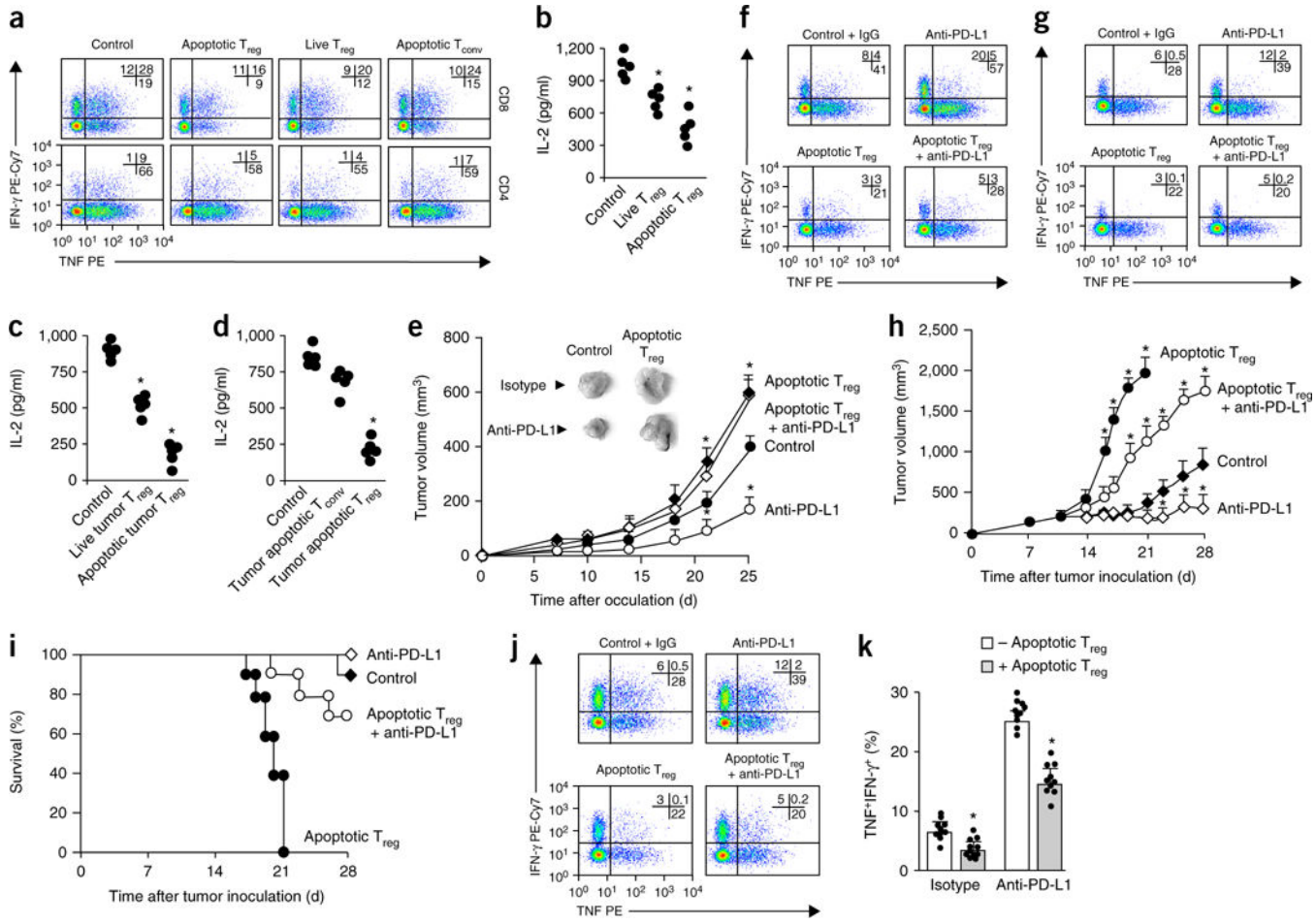

Figure 2.

Apoptotic T_{reg} cells are immunosuppressive. (**a**) Immunosuppression mediated by human ovarian-cancer-associated apoptotic T_{reg} cells. $CD3^+CD4^+CD25hi$ T_{reg} cells were enriched and sorted from fresh ovarian cancer tissues. We used anti-Fas mAb to induce apoptosis in T_{reg} cells and conventional T (T_{conv}) cells. Apoptotic T_{reg} cells, live T_{reg} cells, and apoptotic T_{conv} cells were cultured with T cells at a ratio of 1:2 in the presence of anti-CD3 and anti-CD28. Shown are representative results of flow cytometry analysis of the expression of IFN-γ and TNF in $CD4^+$ and $CD8^+$ T cell gates. (**b**) Immunosuppression by human ovarian-cancer-associated live T_{reg} cells and apoptotic T_{reg} cells. We measured T cell IL-2 by ELISA on day 3. (**c**) Immunosuppression mediated by mouse MC38-associated live and apoptotic T_{reg} cells. Mouse GFP^+Foxp3^+ T_{reg} cells were sorted from MC38 tumor tissues and treated with anti-Fas mAb to induce apoptosis. T cell immunosuppressive assays included equal numbers of live T_{reg} cells and apoptotic T_{reg} cells. We measured T cell IL-2 by ELISA on day 3. (**d**) Immunosuppression mediated by mouse MC38-associated apoptotic T_{reg} cells and apoptotic conventional T cells. Mouse GFP^+Foxp3^+ T_{reg} cells and GFP^-Foxp3^- T cells were enriched and sorted from MC38 tumor tissues and treated with anti-Fas mAb to create apoptotic T_{reg} cells and conventional T cells. T cell immunosuppressive assays included equal numbers of apoptotic T_{reg} cells and apoptotic conventional T cells. We measured T cell IL-2 by ELISA on day 3. In **b,c,d**, each individual data point represents a single donor

($n = 5$), and significant differences are relative to the control. (**e**) The effect of apoptotic T_{reg} cells on MC38 tumor growth *in vivo*. C57BL/6 mice were inoculated subcutaneously with MC38 tumor cells or MC38 tumor cells plus radiation-induced apoptotic T_{reg} cells. On days 7 and 14 the mice were treated with anti-PD-L1 or isotype control antibody. Tumor volume was measured at the indicated time points. The images in the upper left show representative tumors at the endpoint of the experiment. Data shown are the mean and s.d. from $n = 10$ mice per group. (**f,g**) Cytokine expression as measured by flow cytometry in tumor-draining lymph nodes (**f**) and tumor tissue (**g**) at the endpoint of the experiments. The cells were gated on the $CD45^+CD3^+$ population. $n = 5$ mice per group. (**h,i**) The effect of apoptotic T_{reg} cells on B16-F10 tumor growth in a TAA-specific T cell transfusion model. Experiments are described in Supplementary Figure 6g. *Rag2*$^{-/-}$ mice were inoculated subcutaneously with B16-F10 cells, and after 7 d PMEL-specific T cells were transferred intravenously. Mice received intratumoral T_{reg} cells and mAb treatment. Tumor growth (**h**) and mouse survival rate (**i**) were monitored. The data in **h** are the mean ± s.d. of $n = 10$ mice per group. Survival curves with initial animal numbers were considered as 100% (**i**). (**j,k**) The effect of apoptotic T_{reg} cells on effector cytokine expression in PMEL-specific T cells. We used flow cytometry to analyze cytokine expression in tumor-infiltrating $CD45^+CD3^+CD8^+$ T cells. Data are presented as representative dot plots (**h**) and quantification of polyfunctional $TNF^+IFN\text{-}\gamma^+$ populations (**i**). The data in **i** are the mean and s.d. of $n = 10$ mice per group. Data are from 4 experiments (**a**), 1 experiment with 5 donors (**b**–**d**), or 1 experiment with 10 animals per group (**e**–**k**). In **a,f,g,j**, numbers in upper right corners show the percentage of cells in the indicated quadrants. PE, phycoerythrin; Cy7, indotricarbocyanine. $*P < 0.05$ versus control, Wilcoxon test (**b,d**) or Student's *t*-test (**c,e,h,k**).

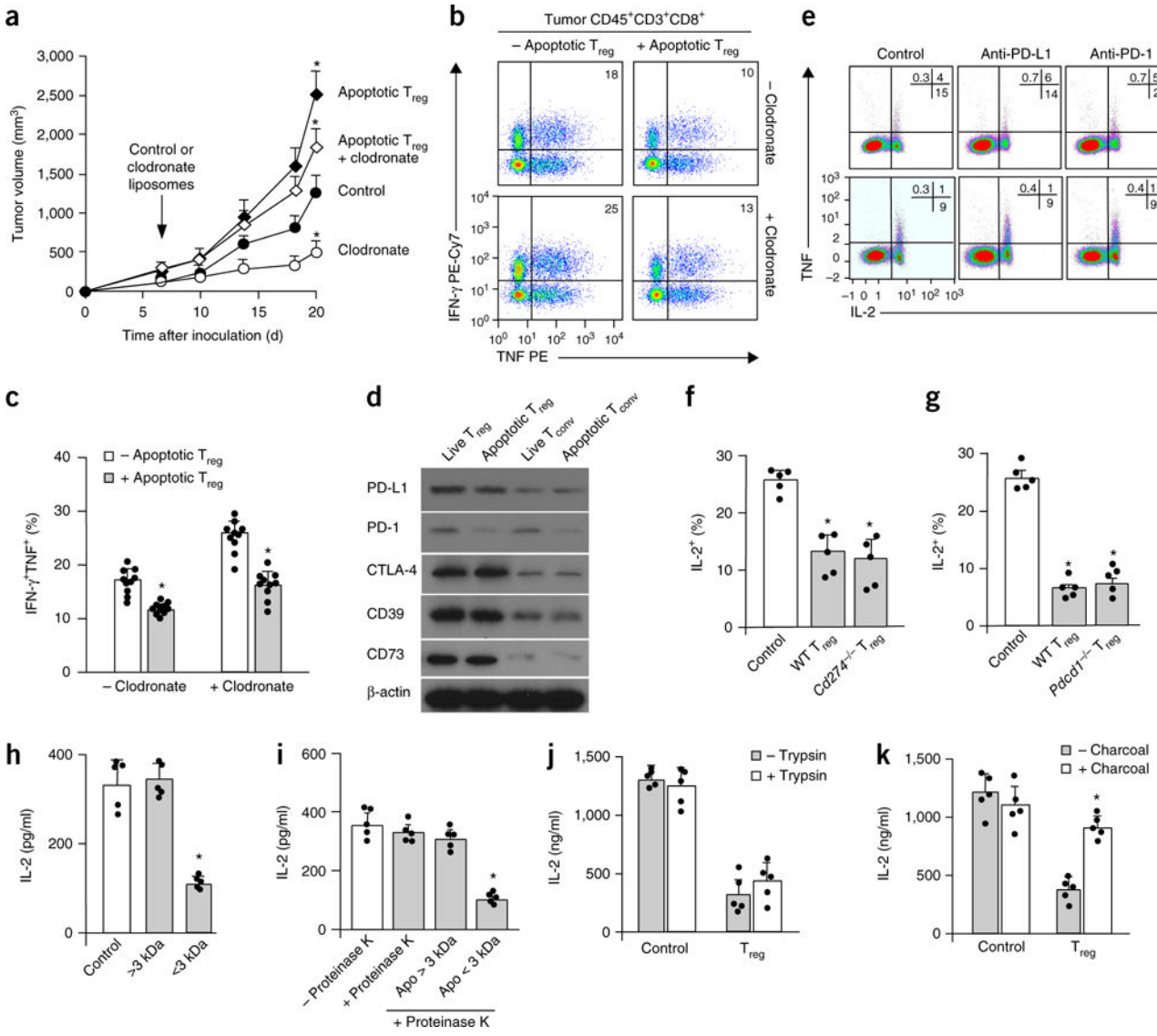

Figure 3.

Apoptotic T_{reg} cells mediate immunosuppression via soluble factor(s). (**a**–**c**) The effect of macrophage depletion on apoptotic T_{reg} cell–mediated suppression. Mice bearing MC38 and apoptotic T_{reg} cells were treated with clodronate-loaded liposomes. The plots show tumor volume (**a**) and numbers of tumor-infiltrating effector T cells (**b,c**). Data in **a** and **c** are the mean and s.d. of $n = 10$ mice per group. $^*P < 0.05$ versus the control, Student's t-test. (**d**) The expression of immunosuppression-associated molecules in live and apoptotic T cell subsets. The indicated mouse T cell subsets were immunoblotted with antibodies to the indicated proteins. (**e**) The effect of PD-L1 or PD-1 blockade on apoptotic T_{reg} cell–mediated T cell suppression. Apoptotic T_{reg} cells and apoptotic conventional T cells were induced by irradiation. Apoptotic T_{reg} cells and apoptotic conventional T cells were cultured with normal T cells at a ratio of 1:2 in the presence of anti-CD3. We measured the expression of T cell TNF and IL-2 by flow cytometry. (**f,g**) Immunosuppression mediated by PD-L1$^-$, PD-1$^-$, and wild-type (WT) apoptotic T_{reg} cells. Apoptotic T_{reg} cells from

Cd274$^{-/-}$ (**f**), *Pdcd1*$^{-/-}$ (**g**), and wild-type mice were cultured with normal T cells at a ratio of 1:2 in the presence of anti-CD3. We measured the expression of T cell TNF and IL-2 by flow cytometry. Data shown are the mean and s.e.m. ($n = 5$ mice). *$P < 0.05$ compared with controls, Wilcoxon test. (**h**) Immunosuppression mediated by low-molecular-weight components in apoptotic T_{reg} cell–derived supernatants. T_{reg} cells were treated with anti-Fas mAb for 6 h. T_{reg} cell supernatants were passed through a 100-kDa cutoff filter and divided into two fractions with a 3-kDa cutoff filter. The two fractions were collected for T cell immunosuppression assays. T cell IL-2 was detected on day 3 by ELISA. The data shown are the mean and s.d. ($n = 5$ mice). *$P < 0.05$ versus the control, ANOVA with Dunett's post-test. **(i,j)** Immunosuppression mediated by nonprotein elements in apoptotic T_{reg} cell supernatants. Apoptotic T_{reg} cell supernatants (apo) were treated with proteinase K (**i**) or trypsin (**j**) and subsequently used for immunosuppression assays. T cell IL-2 was detected on day 3 by ELISA. The data shown are the mean and s.d. ($n = 5$ mice). ANOVA with Dunett's post-test, *$P < 0.05$. (**k**) The effect of the removal of small lipid-like factors on immunosuppression mediated by apoptotic T_{reg} cell supernatants. Apoptotic T_{reg} cell supernatants were mixed with charcoal-treated dextran to remove small lipid-like molecules and were subsequently used for immunosuppression assays. T cell IL-2 was detected on day 3 by ELISA. The data shown are the mean and s.d. ($n = 5$ mice). Wilcoxon test, *$P < 0.05$ versus the control. Data are representative of 10 (**d**) or 5 (**e**) experiments. In **b** and **e**, numbers in the upper right show the percentage of cells in the indicated quadrant.

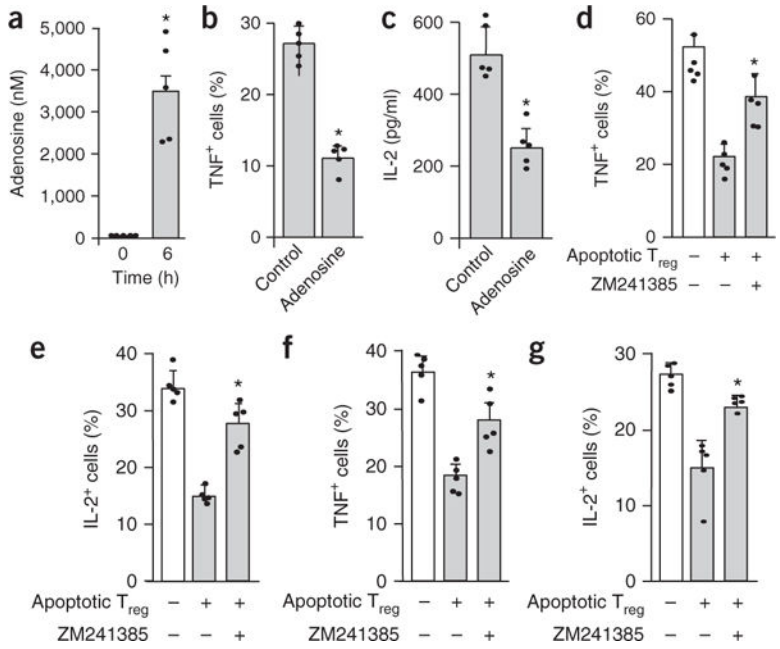

Figure 4.

Apoptotic T_{reg} cells mediate immunosuppression via adenosine. (**a**) Adenosine in apoptotic T_{reg} cell supernatants. Mouse T_{reg} cells were treated with anti-Fas mAb for 6 h. (**b,c**) The effect of exogenous adenosine on T cell TNF (**b**) and IL-2 (**c**) expression. Mouse T cells were activated with anti-CD3 and anti-CD28 in the absence (control) or presence of adenosine (5 μM). T cell cytokines were analyzed by flow cytometry on day 3. (**d,e**) The effect of the A_{2A} inhibitor ZM241385 on mouse apoptotic T_{reg} cell–mediated immunosuppression. Mouse T cells were activated with anti-CD3 and anti-CD28 in the presence of apoptotic T_{reg} cell supernatants for 3 d. ZM241385 was added into the culture. Expression of the T cell cytokines TNF (**d**) and IL-2 (**e**) was analyzed by flow cytometry on day 3. (**f,g**) The effect of ZM241385 on human cancer-associated apoptotic T_{reg} cell–mediated immunosuppression. Human T cells were activated with anti-CD3 and anti-CD28 in the presence of human ovarian-cancer-associated apoptotic T_{reg} cell supernatants for 3 d. ZM241385 was added into the culture. Expression of the T cell cytokines TNF (**f**) and IL-2 (**g**) was analyzed by flow cytometry on day 3. All data are representative of 1 experiment with cells acquired from 5 different animals and are shown as the mean and s.d. of $n = 5$ mice.*$P < 0.05$, paired Student's *t*-test (**a**–**c**) or ANOVA with Dunett's post-test (**d**–**g**). In **d**–**g**, significant differences are versus the untreated control group.

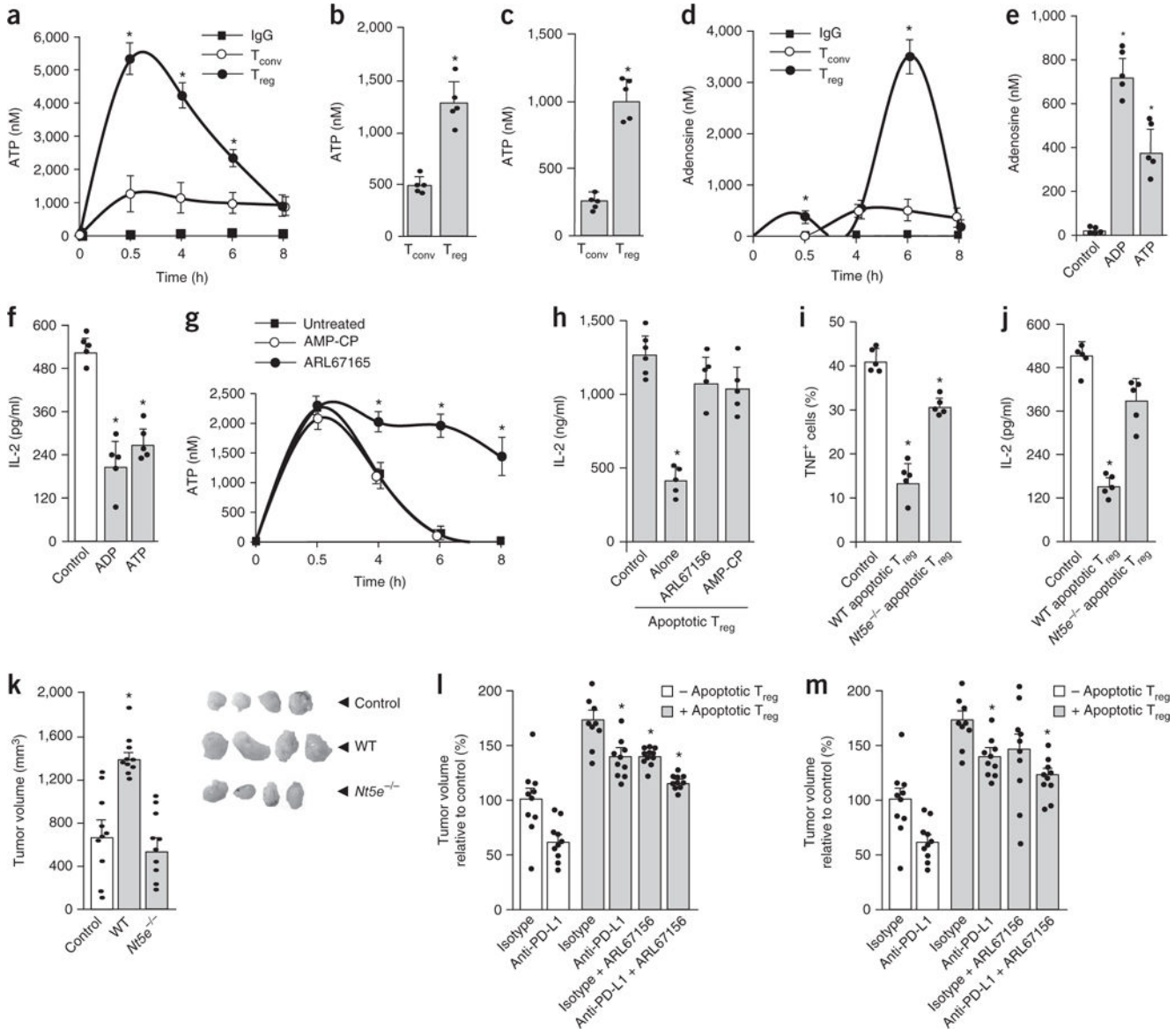

Figure 5.

Apoptotic T_{reg} cells release ATP and generate high levels of adenosine. (**a**) Kinetics of ATP release by apoptotic T_{reg} cells. Mouse T_{reg} cells and conventional T cells (T_{conv}) were treated with anti-Fas mAb or isotype IgG. ATP in the supernatant was measured by colorimetric assay. Mean ± s.d., $n = 6$. $^*P < 0.05$, Student's *t*-test between T_{reg} cells and conventional T cells at each time point. (**b,c**) ATP released by mouse apoptotic T_{reg} cells under serum starvation (**b**) or after irradiation (**c**) in the presence of ectonuclease inhibitor ARL67156. The ATP concentration in apoptotic T_{reg} supernatants was measured at 16 h. Mean and s.d., $n = 5$. $^*P < 0.05$, Student's *t*-test. (**d**) Kinetics of adenosine generation by apoptotic T_{reg} cells. Mouse T_{reg} cells and conventional T cells were treated with anti-Fas mAb or isotype IgG in the presence of the adenosine deaminase inhibitor EHNA. Adenosine was measured in the supernatant. Mean ± s.d., $n = 6$. $^*P < 0.05$, Student's *t*-test between T_{reg} cells and conventional T cells at each time point. (**e,f**) Adenosine generated from exogenous

ADP and ATP by apoptotic T_{reg} cells. Exogenous ADP or ATP (5 μM) was added to fresh medium with apoptotic T_{reg} cells for 6 h. Adenosine was measured in the culture supernatants (**e**). Supernatants were used for immunosuppression assays (**f**). Mean and s.d., $n = 5$. $^*P < 0.05$ versus control, Wilcoxon test. (**g**) The effect of ARL67165 or AMP-CP on ATP release by apoptotic T_{reg} cells. Mouse T_{reg} cells were treated for 8 h with anti-Fas mAb with or without ARL67165 or AMP-CP. ATP was measured in the supernatants. Mean ± s.d., $n = 5$. $^*P < 0.05$ versus the untreated control, Wilcoxon test. (**h**) The effect of ARL67165 or AMP-CP on apoptotic T_{reg} cell–mediated immunosuppression. Mouse T_{reg} cells were cultured for 8 h with anti-Fas mAb with or without ARL67165 or AMP-CP. The culture supernatants were used for T cell immunosuppression. IL-2 was measured on day 3 by ELISA. Mean and s.d., $n = 8$. $^*P < 0.05$ versus control, ANOVA with Dunett's post-test. (**i,j**) Immunosuppression mediated by wild-type (WT) and *Nt5e*$^{-/-}$ apoptotic T_{reg} cells. Apoptotic T_{reg} cells from wild-type and *Nt5e*$^{-/-}$ mice were used for T cell immunosuppressive assays. TNF expression was measured by flow cytometry (**i**), and IL-2 was detected by ELISA (**j**). Mean and s.d., $n = 5$. $^*P < 0.05$ versus control, Wilcoxon test. (**k**) The effect of *Nt5e*$^{-/-}$ apoptotic T_{reg} cells on tumor growth *in vivo*. MC38 tumors were inoculated subcutaneously with wild-type or *Nt5e*$^{-/-}$ apoptotic T_{reg} cells. The images show representative tumors at the endpoint of the experiment. Mean and s.e.m., $n = 10$. Student's *t*-test, $^*P < 0.05$ versus control. (**l,m**) The effects of CD39 and A_{2A} inhibitors on tumor growth. MC38-bearing mice were treated with the CD39 inhibitor ARL67165 (5 mg/kg, 5 d per week) or the A_{2A} inhibitor ZM241385 (1 mg/kg, 5 d per week) with anti-PD-L1 in the presence of apoptotic T_{reg} cells. Mean and s.e.m., $n = 10$. $^*P < 0.05$ compared with isotype control in the presence of the apoptotic T_{reg} cell group, ANOVA with Dunnett's *post hoc* test. All data in **a**–**j** were generated in single experiments; *n* values for those panels indicate the number of animals used for cell isolation. Data in **k**–**m** are from 1 experiment with 10 animals per group.

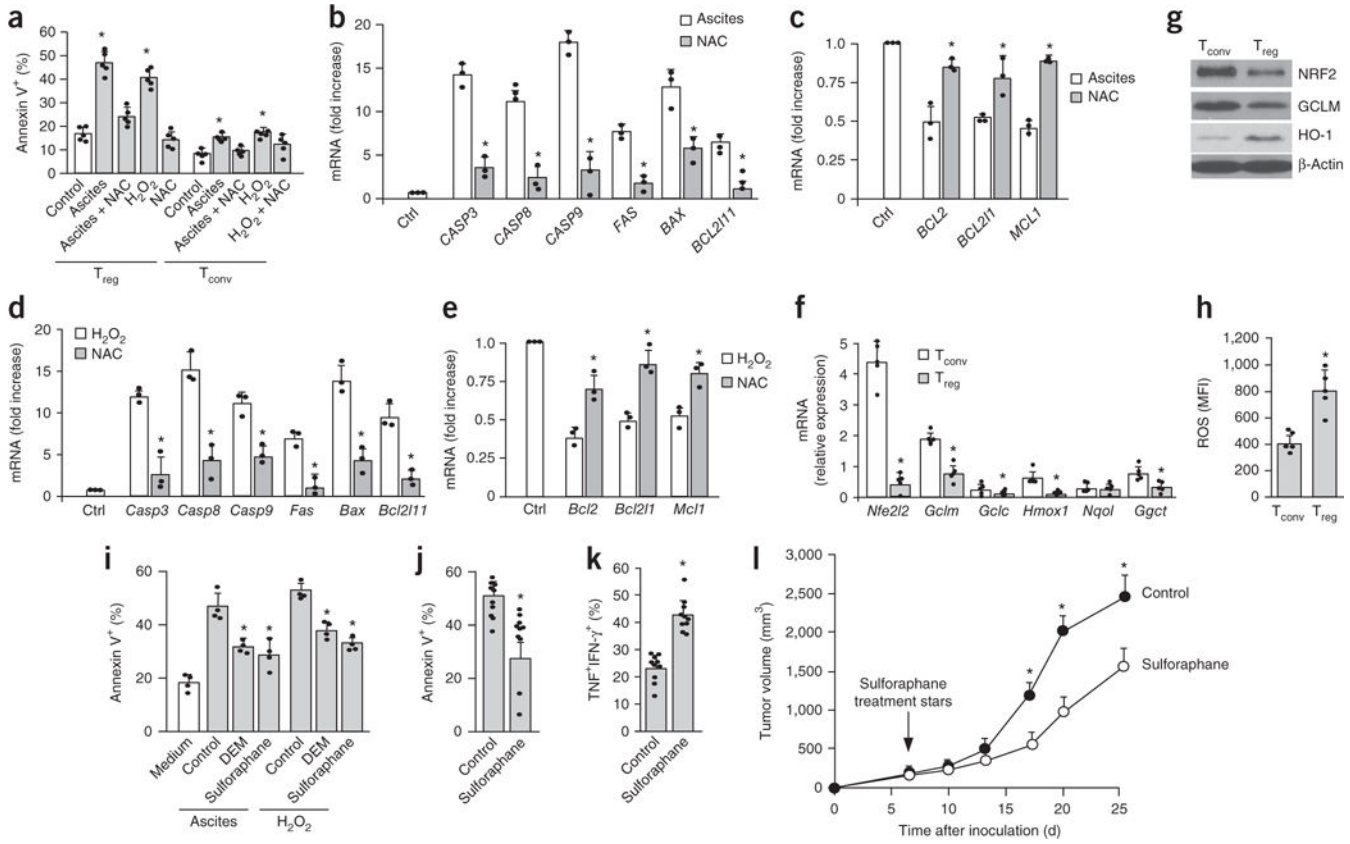

Figure 6.

Oxidative stress induces T_{reg} cell apoptosis in the tumor environment. (**a**) The effect of ovarian cancer ascites on human T_{reg} cell apoptosis. Mouse T_{reg} cells and conventional T cells (T_{conv}) were cocultured with 50% human ovarian cancer ascites or hydrogen peroxide for 24 h. Additional cultures were treated with *N*-acetyl-cysteine (NAC) as a free radical scavenger. Annexin V^+ T_{reg} cells and T_{conv} cells were analyzed by flow cytometry. $n = 5$. (**b,c**) The effect of ovarian cancer ascites on proapoptotic and antiapoptotic gene transcripts in T_{reg} cells. T_{reg} cells were exposed to ascites or ascites plus NAC after 24 h. Proapoptotic (**b**) and antiapoptotic (**c**) transcripts were quantified by real-time PCR. $n = 3$. (**d,e**) The effect of hydrogen peroxide on proapoptotic and antiapoptotic transcripts in T_{reg} cells. T_{reg} cells were exposed to hydrogen peroxide or hydrogen peroxide plus NAC after 24 h. Proapoptotic (**d**) and antiapoptotic (**e**) mouse gene transcripts were quantified by real-time PCR. $n = 3$. (**f,g**) Expression of mouse NRF2 and NRF2-associated gene transcripts (**f**) and proteins (**g**) in T cell subsets as determined by real-time PCR and immunoblotting, respectively. $n = 5$. (**h**) The expression of intracellular ROS in T_{reg} cells. T_{reg} cells and conventional T cells were cultured overnight. Amounts of intracellular ROS were measured by flow cytometry. $n = 5$. MFI, mean fluorescence intensity. (**i**) The effect of NRF2 inducers on T_{reg} cell apoptosis *in vitro*. Mouse T_{reg} cells were cultured for 24 h with 50% ascites or medium containing H_2O_2. NRF2 inducers diethylmaleate (DEM; 100 μM) and sulforaphane (10 μM) were added to the culture for 24 h. Controls were treated with vehicle (DMSO). Apoptosis was measured by flow cytometry with annexin V. $n = 4$. (**j–l**) The effect of sulforaphane on tumor immunity. MC38-bearing mice were treated with sulforaphane (25 mg/kg, 5 d per

week) or vehicle (DMSO). Tumor T_{reg} cell apoptosis (**j**) and $CD8^+$ T cell polyfunctional cytokine expression (**k**) were analyzed by flow cytometry. Tumor volume was monitored (**l**). $n = 10$. All data are shown as the mean and s.d. and are from 1 experiment with 10 animals per group (**i**–**l**) or from single experiments with cells isolated from individual animal for each data point (**a**–**h**). $*P < 0.05$ versus control, Wilcoxon test (**b**–**e**), paired Student's *t*-test (**f,g**), Student's *t*-test (**i**–**l**), or Mann–Whitney *U*-test (**a,h**).